TRIBOLOGICAL PROPERTIES OF DIFFERENT SLIPPER DESIGNS OF AN AXIAL PISTON PUMP

Svenja Horn[1]*, Roman Ivantysyn[1], Torsten Schmidt[2], Jürgen Weber[1], Jörg Schneider[2]

[1]*Institute of Mechatronic Engineering, Technische Universität Dresden, Helmholtzstrasse 7a, 01069 Dresden*
[2] *Fraunhofer-Institut für Werkzeugmaschinen und Umformtechnik, Reichenhainer Straße 88, 09126 Chemnitz*

* Corresponding author: Tel.: +49 351 463-33701; E-mail address: svenja.horn@tu-dresden.de

ABSTRACT

New application areas such as compact drives and displacement control using variable electric motors require that hydrostatic machines exhibit good performance also at very low relative speeds without being damaged during critical mixed friction conditions. While some pumps currently address this issue using leaded metals in their sliding bearings, European regulations (Reach Regulation) mandate the transition to lead-free materials in the near future. To address these challenges, this paper investigates about surface structures that offer the ability to selectively modify the pressure field within the fluid gap, generating additional hydrodynamic pressure. In this research project, various slipper surface structures of an axial piston pump were developed through extensive simulation studies and tested on a pump test-rig as well as on a dedicated hydrostatic tribometer.

This paper outlines the development, construction, and optimization of a novel hydrostatic tribometer capable of adjusting speed, pressure, acceleration and temperature. Multiple measurements were conducted with different slipper geometries. The results encompass torque, temperature and wear measurements. They are presented along with a comprehensive analysis and validation of the findings in comparison to simulation and pump test results. In this study the tribometer revealed specific constraints not detected in pump bench tests, underscoring the imperative nature of such examinations.

Keywords: Tribometer, Slippers, Surface, Tribology, Wear

1. INTRODUCTION

The increasing electrification of hydraulic systems poses new operational speed challenges for hydrostatic pumps. Specifically, at lower speeds, these pumps need to sustain loads without succumbing to mixed friction and wear. Presently, some pumps can handle these conditions, largely due to their use of leaded metals in their sliding bearings. These metals are proficient at withstanding critical contact scenarios. However, the shift towards lead-free materials is imminent to align with European standards (Reach Regulation). Previous research has shown that surface structures can improve the tribological characteristics of hydrostatic bearings [1]. Meso-structures refer to surface patterns with slight height variations (in the µm range) spread over broader areas (in mm). Such structuring can selectively alter the fluid gap's pressure field, leading to an enhanced performance.

In previous publications, [2], [3] and [4] such structures were designed and tested for a slipper of an axial piston pump. The optimization method and pump measurements of a wave and a step surface structure are explained in detail in these publications. Especially the step structure achieved a notable enhancement in the overall pump efficiency when compared with a non-structured flat slipper. A

remarkable feat was the reduction of the pump's start-up torque by an astonishing 80% by integrating the stepped slipper design. This pump underwent rigorous testing on a test bench under challenging scenarios, from start-stop sequences and extremely low speeds (both loaded and unloaded), to cold starts and a demanding endurance test under an elevated pressure. Impressively, the slippers weathered these tests with negligible wear of less than one micrometer. Nevertheless, to truly gauge the potential constraints of different slipper designs, a more streamlined component test is essential.

In conventional pump measurements on a laboratory system test bench, it is very time consuming to remove the slippers for wear measurements or to completely change them in order to compare the performance of different designs and materials. Furthermore, it is impossible to investigate only the slipper/swashplate tribo-contact without including the losses of the other sealing gaps. Tribometer evaluations stand out for their ability to test the sliding and frictional attributes of various designs in isolation. The aim of the presented work is to investigate on different slipper designs and materials and their performance at different testing conditions, bypassing the lengthy procedures associated with pump test rigs. The difficulty in designing a suitable tribometer is to keep the set-up as simple as possible while still providing realistic results. Such as standard tribometers often renounce the hydrostatic pressure field within the slipper pocket, a pivotal mechanism that is essentially determining the performance of the lubricating interfaces [5]. This disadvantage will be overcome with the herein presented hydrostatic tribometer set-up.

Chapter 3 of this paper shows how a commercially available tribometer can be adapted with hydrostatics to explore the tribological properties of the slipper/swashplate interface. It describes the challenge to choose a good compromise between keeping the test-rig set-up simple while achieving useful results. The hydrodynamic performance of the different meso-structured slipper designs is investigated by torque measurements over a broad speed spectrum and several pressures in chapter 4. The advantages of the capabilities of such a tribometer, as compared to a full pump test rig, were highlighted by the effects of thermal deformation on the performance of the slipper. Those are described in chapter 5, also including ANSYS® simulations to reveal the underlying physical mechanisms.

2. STATE OF THE ART

For the reasons mentioned above, the focus in the next section will be on functional slipper test rigs that allow for easy slipper replacement. Those test rigs can be categorized into four distinct types, as illustrated in **Figure 1**, with complexity escalating from left to right. The initial type (a) features both a stationary slipper and swash plate, a setup employed by Manring to measure the pressure beneath the slipper sealing, as referenced in [6]. Such a configuration facilitates the integration of a wide array of sensors, eliminating the need for telemetry systems or load-resistant bearings, but at the cost of overlooking component movement. Conversely, the second category of tribometer (b) introduces a rotating disc accompanied by one or more hydrostatically supported slippers. This approach is selected for the herein developed tribometer, primarily because it subjects the bearings only to axial stresses, thereby simplifying the rotational assembly. The first empirical investigations on such a test rig was done by Renius in 1973 [7]. These were the first isolated slipper efficiency measurement tests, accomplished by recording both the frictional forces and leakages for a single slipper. It is noteworthy that this set up also included pulsating high pressure using a valve. Next to efficiency the publications also featured the Stribeck curve for slippers for different balancing ratios. Many other researchers used the type (b) set up, as it recreates a quiet realistic test environment to evaluate slipper performance mainly by measuring friction and leakage [8–11]. The stationary slippers allow for interesting sensor placement for example temperature [12, 13], pressure [10] or displacement sensors to measure the micro movement and gap height [14–16].

A few studies have also been performed on a wobble plate type set up, which is the closest set up one can chose before rotating the slippers. Notably Iboshi used such a set up and still measured the displacement of the slippers, however while prohibiting slipper spin [17]. That the slipper spin is important and existing was shown by Bergada [10] and then later measured in a type (d) test rig by Chao [18].

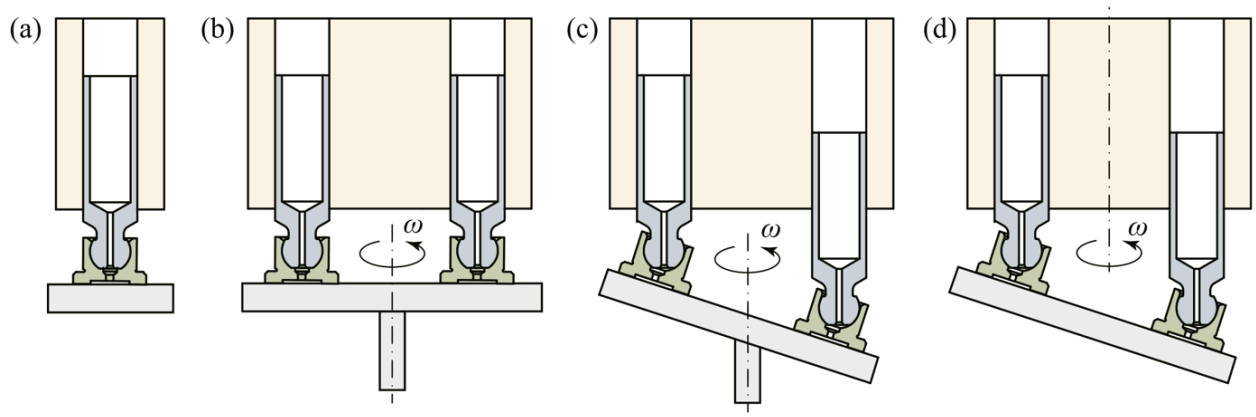

Figure 1: Types of slipper test rigs [19]

This section presents the most relevant research on functional slipper test-rigs. For a complete review of slipper test rigs published in the last 50 years, the work of Chao can be recommended [20]. A previously uncharted territory, however, is the goal to retrofit a commercially available tribometer with hydrostatic capabilities, all the while retaining the original rotating components, block, piston, and slipper, in their unmodified form. While this methodology seems economically favorable for those already equipped with a tribometer, it's not devoid of challenges, as explained in this paper.

3. DEVELOPMENT OF A HYDROSTATIC TRIBOMETER

3.1. Adaption of an existing rotary tribometer to hydrostatics

A concept has been developed to accommodate the original pump components of the swash plate/slipper friction pairing for hydrostatic testing in a hydrostatic tribometer environment. This enables an isolated friction measurement to be conducted, without any influence from other parts of the power unit. The specifications for slipper testing have been set to a maximum load of 300 bar and a rotating speed of up to 2300 rpm. The implementation is based on a TRM 5000 rotary tribometer from Wazau, shown in the photo in **Figure 2**. A new spindle has been added to the tribometer's basic structure to accommodate axial loads of up to 12 kN, in order to realize the test specifications. This axial load limits the number of pistons to one, a compromise that was accepted in order to reach high pressures. However, this in turn means that there is a very high asymmetric load impact on the tribometer frame, producing a tilting of the system. The system has been blocked and stabilized as good as possible reducing the tilting from over 150 µm to 20-40 µm in x and y-direction. To measure force and torque a Kistler Type 9265A 3-component dynamometer was used in combination with a multichannel Kistler charge amplifier Type 5080A1088004. Operating pressures up to 300 bar are provided by a separately controllable "Cytrobox" hydraulic unit from Bosch Rexroth. The original swashplate is substituted by a plate with rotational symmetry made of identical material, possessing identical hardness characteristics and sharing the same finish as the original. While the block and the slippers rotate in an axial piston pump, the presented tribometer setup includes a rotating swashplate. This setup offers the advantage of solely having the slipper / swashplate pairing's sliding interface present, without any influences from the valve plate or the piston sealings. The slipper is employable in its original form in the tribometer.

Figure 2 illustrates the assembly of the components and the adaptation of the pressure supply line. The role of the block holder is to connect the block and hydraulic hose, and channel hydraulic oil from the hose into the cylinder chamber of the block where the piston is located. The hose is connected using a quick release coupling. To seal the interface between the block holder and the block, a copper seal with an aperture for filling a cylinder chamber is used. The seal is secured tightly with eight M6 screws and one M14 screw.

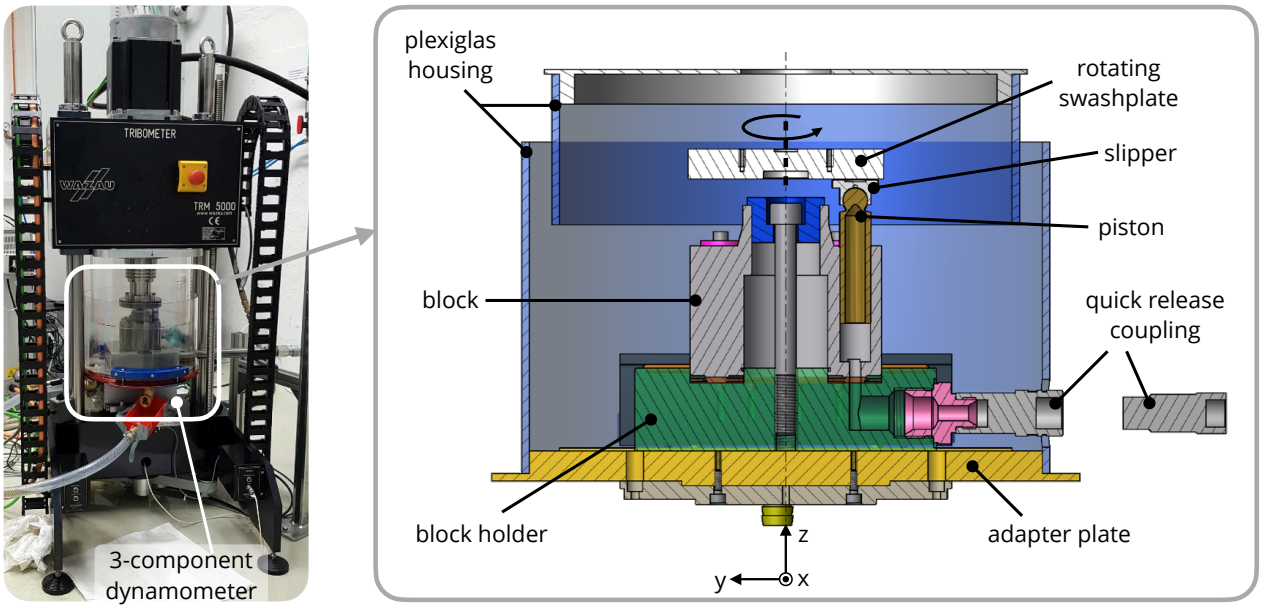

Figure 2: Tribometer set-up (left) and components of the new hydrostatic adaption (right)

The optimal hose routing was established through preliminary tests to minimize the impact of hydraulic hose supply lines on measured torque. The weight, position, and bending radius of the hose can affect the measuring system. The most effective hose guidance was determined in static tests without rotating the swashplate. To prevent oil leakage, a Plexiglas housing has been installed. Leakage oil can be drained from two oil drain holes and pumped back to the CytroBox oil tank through a 10 µm filter using an oil level-controlled pump. Additionally, the leakage oil drain is separated from the return lines, preventing any torque influence. To avoid a sudden impact of the slipper surface on the swashplate surface during pressure build-up, a compression spring has been inserted into the block bore. This indicates that the surfaces of the test pair are in contact with a very low preload of approximately 50 N before the pressure builds up and impact is avoided. The tribometer is PC-controlled using the "TriboControl V11" software. The CytroBox is controlled using "IndraWorks DS". The measurement of the forces and moments using the 3-component dynamometer are recorded with "imc Studio".

3.2. Measurement set-up

One of the greatest difficulties of the measurement setup is to measure very low friction values in the x-y plane as accurately as possible, despite the extremely high forces due to the piston pressures in the z-plane in the range of several kN. Ideally, the torque should be measured directly at the disc, as close as possible to the friction point. However, this in turn means that there must be a suitable bearing of the high axial forces that does not cause any additional frictional forces. Since a corresponding set-up was not available, a force measurement platform from Kistler was used, which is mounted under the block (see **Figure 2**). The high-precision quartz force sensors installed in it can be adjusted in their measuring range between 0-1.5 kN or 0-3 kN, whereby the smaller measuring range is selected for the x-direction of the measured force that is relevant for the torque calculation.

After numerous optimization loops, a pressure-dependent offset of the forces to be measured remains,

which can be traced back to the tilting of the tribometer frame mentioned in the previous paragraph and a sensor-specific crosstalk. To account for this, an initial right/left-wise rotation combination at 100 or 500 rpm is carried out at the beginning of each pressure level. The mean value of the respective moments is then used as the offset. In order to achieve a similar lubrication and temperature behaviour to that of the pump, an oil and air cooling system is installed as shown in **Figure 3** (left). It sprays oil in room temperature onto the swash plate and slipper and can also be switched off to overheat the slipper. A pyrometer measures the temperature through a hole in the plexiglass (**Figure 3** middle) on one spot on the disc (**Figure 3** right) before or after the slipper passes that position, depending on the rotating direction.

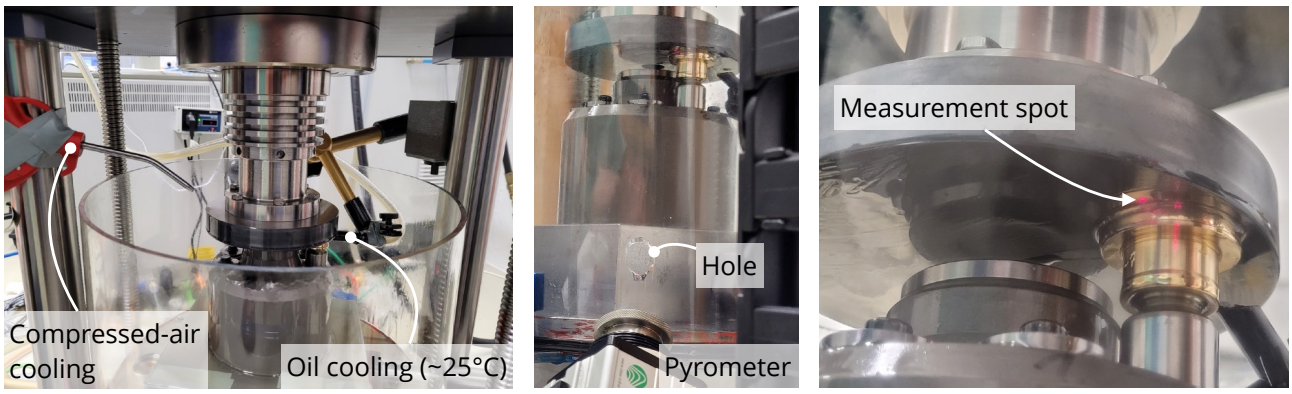

Figure 3: Set-up of the compressed-air and oil cooling of the slipper / disc interface

3.3. Investigated slipper designs

Figure 4 shows the slippers studied in this investigation. They were optimized and developed through simulation, explained in detail in [3]. All designs have the same outer radius of 29.6 mm but different inner radii and thus a different hydrostatic lift capacity. The reference design (left) is a flat, single land slipper design with an optimized balance factor of 99 %. The balance factor is an indicator of the slipper's pocket size and is given in (1). It is calculated by dividing the hydrostatic force F_{fz}, that is estimated as logarithmic pressure drop over the sealing land, by the force of the piston on the slipper F_{AK}, multiplied by the cosine of the swashplate angle β:

$$B = \frac{F_{fz}}{F_{AK}} \cdot cos\beta \tag{1}$$

Figure 4: investigated slipper designs and their optimized micro structure

The wave design (middle) contains a sine-wave micro structure on the sealing land with an amplitude of ±3 µm and a balance of 102.3 %. The paper presents results on wave design only for pump

measurements. Tribometer results with wave slipper can be found in [21]. The design of the step slipper (right) features a step down of 6 µm towards the external radius, located approximately midway along the sealing land and has the highest balance value of 105 %. The location and magnitude of this step was carefully engineered using advanced numerical simulations as described in [3]. For the manufacturing of the slippers different production processes have been investigated and optimized, documented in [21], whereas a high accuracy drilling has been finally adapted.

Additionally, a slipper with multiple lands has been investigated as it is the current state of the art in industry. Multi-land slippers, also known as slippers with several lands separated by millimeter-deep grooves, provide hydrodynamic lift and stabilize the slipper. The middle land defines the hydrostatic pressure field [22].

3.4. Differences between the hydrostatic tribometer and the pump system

Due to the high complexity of the sealing gaps in the pump, it is not possible to directly compare the measurement results of the tribometer and the pump. Each test scenario has its own advantages and disadvantages and can be used for specific investigations. The following section explains the main differences between the new hydrostatic tribometer set-up and a conventional axial piston pump bench test.

- The tribometer setup uses a rotating swashplate rather than a rotating block, which also requires a second seal on the valveplate side. In this way it is possible to measure only the slipper seal interface. A disadvantage is the lack of centrifugal force that prevents the slippers from tilting. Especially for high speeds, the hydrodynamic lift should be changed compared to the pump system.
- The current tribometer set-up does not include a change between high and low pressure, which can cause the slipper to lift off or tilt due to the sudden change in load. This effect, also known as "breathing", allows the slipper to lift off and reset its tilt, which could also play an important role with regard to the thermal load on the surfaces. For future work an additional control valve could simulate the change in pressure.
- In the pump, the case is filled with oil hence forcing the slippers to run through oil. On the tribometer, an air and oil cooling were installed in order to adapt the lubrication behavior and temperature in the gap between slipper and swashplate. This simplified design allows the temperature to be measured on the swashplate using a pyrometer and the use of a Plexiglass housing to observe the experiment. This set-up allows for an easy replacement of the slipper as well as the usage of different oil types. However, the movement through the oil, as in the pump, could influence the inclination of the slipper and have an enormous cooling effect, which has been underestimated (see chapter 5).
- The swashplate angle on the tribometer is 0° instead of 17° as in the pump for full stroke at 100%. Since the piston does not move axially in the bore, the slipper can be inspected isolated. However, the force balance in formula (1) is changed to a higher value, leading to the assumption that higher gaps occur and thus only a highly reduced friction can be measured between slipper and swashplate. To account for this effect, a “tribometer slipper design” has been developed for each meso-structure through simulation wherein the slipper’s inner diameter has been adjusted to reduce the lift force and balance value. As the tribometer design unexpectedly was subject to excessive wear, the same design as in the pump with a higher balance was selected for most the measurements herein.

4. COMPARISON OF THE SLIPPER DESIGNS USING TORQUE MEASUREMENTS

This section compares the torque losses of the different slipper designs first from measurements of the tribometer and second from results of the full pump test-rig. On the one hand, critical areas are to

be identified and on the other hand, the proportion of the total hydromechanical losses accounted for by the slippers is to be analyzed.

4.1. Tribometer torque measurement results

The aim of the torque measurements was to record the Stribeck curve for the entire speed range from 0-2300rpm for the various slipper designs, being cooled by the external oil and air cooling. This was done by gradually increasing the speed and measuring the torque at steady state. The left plot of **Figure 5** provides the speed and force curves. The left y-axis gives the measured force sensor results in x-direction while the right y-axis shows the speed values, plotted over the samples. At the start and end a +/-500rpm combination for offset calculation has been conducted. The first two curves accelerate from 0 to 2300 rpm with small speed steps in the lower range while the last curve accelerates directly from 0 to 2300 rpm. For each design 0, 50 and 100 bar have been measured twice.

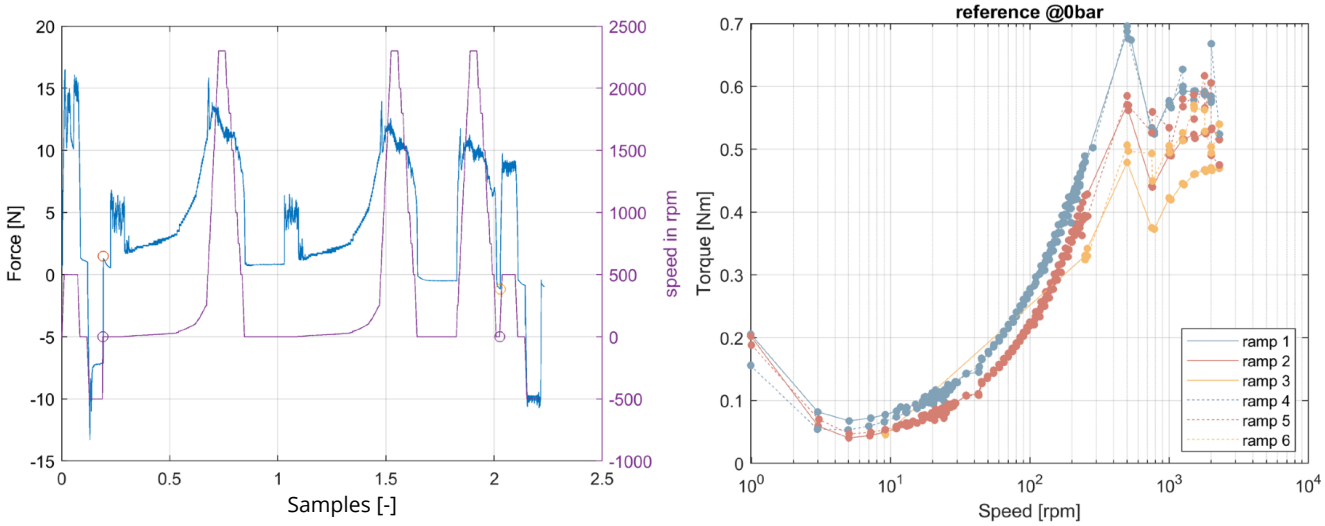

Figure 5: Reference slipper force (left) and torque measurements (right) at 0 bar

As an example for the reference design at 0 bar, the right graph in **Figure 5** shows the derived torque values, based on the measured force for the extracted speed ramps in logarithmic representation. All six speed ramps are plotted for the two trials, the second trial with dashed lines. It is visible that the curves are similar for each ramp especially for speeds below 600 rpm, confirming repeatability of the measurements even at these low forces. As the temperature rises slightly for each ramp the torque losses decrease for this unloaded scenario. This measurement procedure was repeated with the multi-land and step slipper.

Figure 6 shows the torque losses at 0 bar, 50 bar and 100 bar over the speed that is displayed logarithmic and reaching from 0.1 rpm to 2300 rpm for the three different slipper designs reference, multi-land and step. To avoid dynamic effects, the speeds have been measured at steady state and connected in the graph only for reason of clarity. Photos of the surface of each design after testing confirm the results of the torque measurements. For 0 bar, all curves adhere to the Stribeck curve in a qualitative manner. The design with the least friction losses is the step-design and demonstrates significantly better values than alternative designs across all speeds. The torque loss of all designs is at minimum between 5 and 20 rpm and then rise with different slopes. A plateau is reached at approximately 500 rpm, with no notable increase in torque observed for higher speeds for the multi-land and the reference design. As there is no such plateau in the pump measurements in **Figure 7**, the slippers probably are the main contributor to the friction at low pressures, while the other sliding pairings, such as the piston/bushing or block/valve plate, become more significant power loss sources at higher pressures. This is supported by the fact that the replacement of the slipper designs in the

pump significantly changed the low speed performance, while having little effect on the high speed readings, as can be seen in more detail in [4].

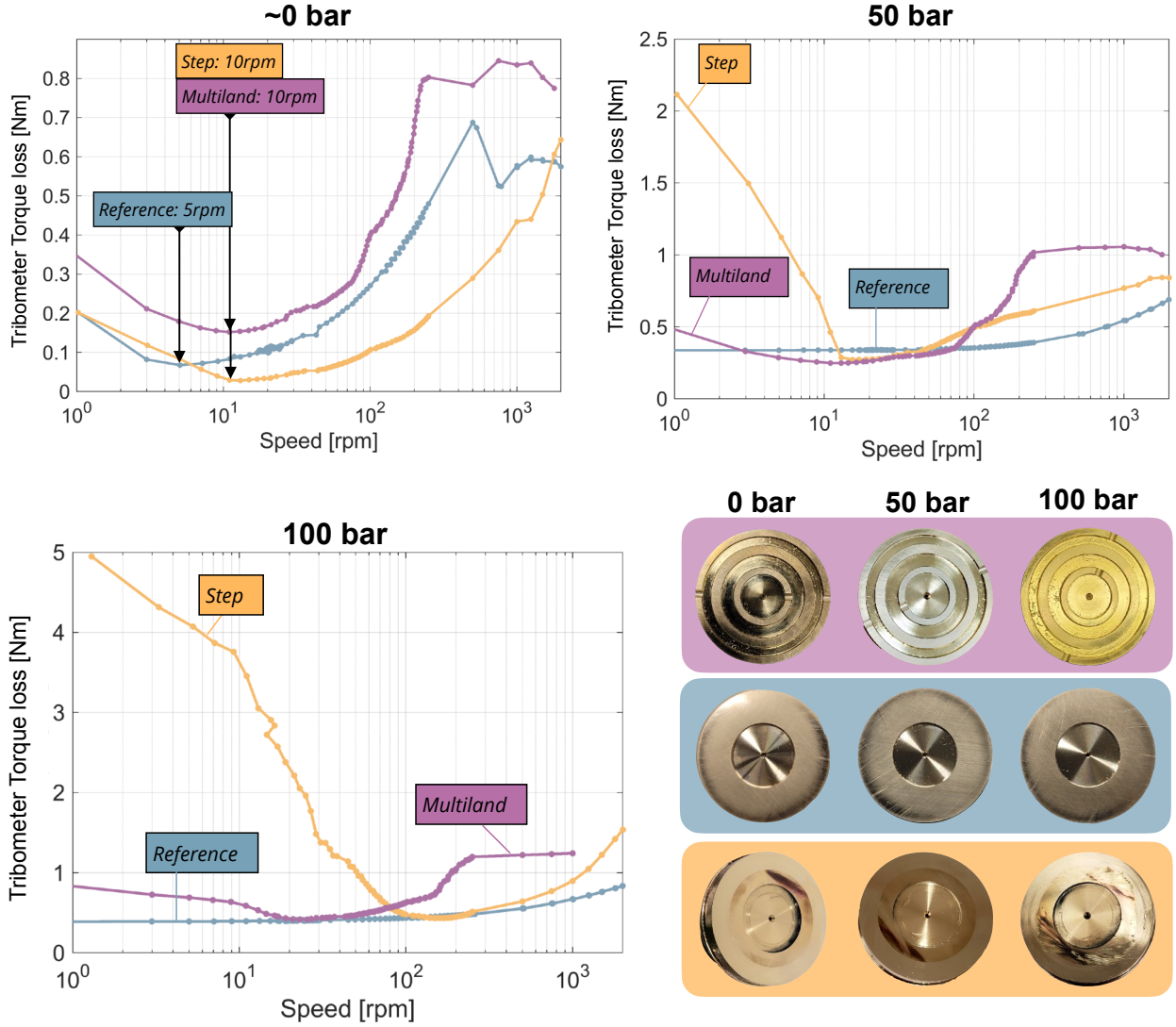

Figure 6: Comparison of tribometer torque loss measurements for 0 bar, 50 bar and 100 bar and a qualitative overview of the wear patterns

Once hydrostatic pressure is built up as for the 50 and 100 bar measurements, the pressure-dependent offset determination is not always reliable. Therefore, the absolute values may vary due to the deformations of the test bench as explained in paragraph 3.4. The qualitative curves of the three designs are very similar for 50 and 100 bar. Quantitatively, the step slipper has twice the friction losses at 100 than at 50 bar, while the reference and the multi-land slipper remain in the same range. The curve of the reference slipper is remarkably flat. At extremely low speeds in the mixed friction range, there is no inclination observed. As anticipated, the slippers are more hydrostatically balanced and "swim" due to the 0° swashplate angle and hence lower piston forces during the tribometer experiment, which leads to lower friction values, especially for low speeds. It is not clear, why the step slipper is not exhibiting the same trend in the low speed region, where it experiences high torques and thus abrasion, even though it has the largest pocket size. One possible explanation is that the step structure is damaged or deformed during the high speed portion at 0 bar, which then has a negative effect on the performance at low speed for 50 and 100 bar. The thermal deformation could play a significant role. The step slipper was shown to have very low leakage and small gap heights, if the temperature is significantly higher at high speed. Consequently, the slipper could also be affected at

low speed, as these measurements are chronologically after the high speed section. That there is serious wear can be seen in the wear patterns of the surface photos. A dark stripe is visible on the inner ring of the surface after 0 bar measurements and smearing of the slipper material after 100 bar measurements.

4.2. Torque measurements of the full pump test bench

Figure 7 shows the torque measurements of the full pump measurement at 0 (left) and 50 bar (right) in a similar presentation to the tribometer Stribeck curves, in order to categorise the torque ranges in which the pump behaves in comparison to the tribometer. The multi-land slipper was not measured in the pump at all speed ranges but the wave slipper and the lead-free step slipper were. While the pump measurements include the torque losses of the entire rotating kit, including the slipper, piston, block and shaft bearings, on the tribometer only one slipper is measured individually. To give a reasonable comparison between the two measurements, the torque losses of the pump were divided by the number of rotating slippers (nine) in order to assess how much just one slipper contributes.

As has been stated earlier, for this pump the slippers seem to be the main contributor of friction at low speed: At 0 bar, the friction losses in the lower speed ranges between 1 - 200 rpm are most likely dominated by the friction losses of the slippers, both ranging from 0 to 0.6 Nm. For higher speeds above 100 rpm, the friction values in the pump increase significantly more for all designs, which could be caused by the losses of the pistons and the valve plate. This trend is even more pronounced at 50 and 100 bar and is in agreement with the simulated analyses in [23], using the same pump. At 50 bar the torque values range from 0.3 Nm to 2.8 Nm exhibited a similar range for both the pump and the tribometer. The qualitative progression of the step curve is quite similar for both tests with a maximum value of just over 2 Nm in the mixed friction area and a minimum friction value of around 0.3 Nm at 10-50 rpm.

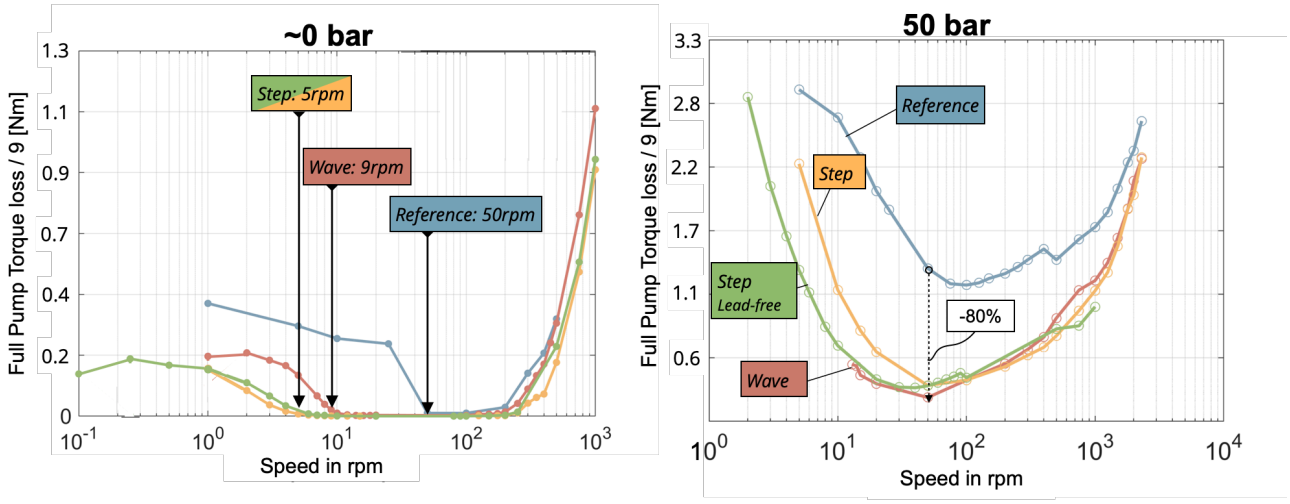

Figure 7: Full pump torque loss divided by 9 for 0 bar (left) and 50 bar (right) over logarithmic speed

While it is clear that the pump and tribometer measurements cannot be directly compared due to higher number of rotating parts in the pump, the overall trends are helpful for an evaluation of the tribometer measurements.

5. EFFECT OF TEMPERATURE ON DIFFERENT SLIPPER DESIGNS

The previous section showed that on the tribometer, the temperature can have a significant effect on slipper performance and wear. Since the pump measurements did not reveal any such trends, the following chapter provides temperature studies from the tribometer and the pump. Paragraph 5.1

presents an overheat test on the tribometer, followed by pump measurements with an increased inlet temperature. Subsequently, the thermal deformation of the slipper is simulated in ANSYS® and the resulting findings are discussed.

5.1. Overheat test using the tribometer set-up

In the following section, the temperature behavior of the step slipper is examined in comparison to the multi-land slipper. The slipper is accelerated three times from 0 to 2300 rpm at 200 bar, in order to introduce a lot of energy into the system. Each maximum speed is held for 5 minutes. A pause of 15 minutes between the ramps was chosen to allow for a cooling-down effect before again introducing energy to the system. **Figure 8** shows the comparison between the step slipper trials with (pink) and without (blue) cooling. While on the left y-axis the temperature is plotted, on the right y-axis the speed is given (orange). For both cases, it is to be expected that the temperature rises during acceleration and the constant speed plateau at 2300 rpm, as these conditions exhibit a great amount of energy into the sliding pair.

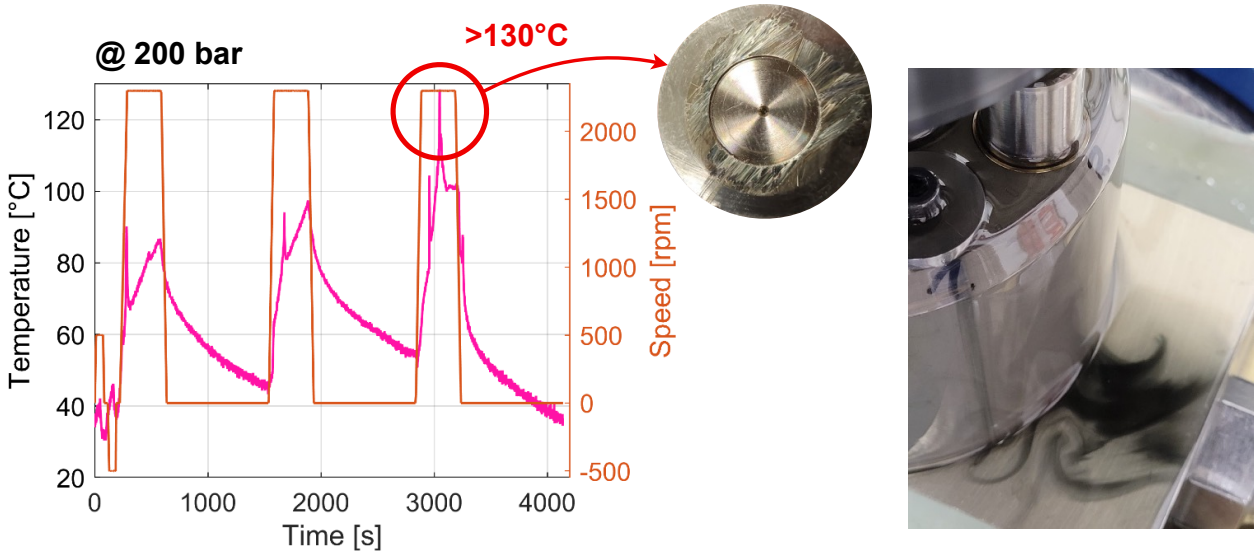

Figure 8: Slipper surface reaches extremely high temperatures and experiences severe wear

The temperatures of the cooled slippers reach less than half the value of the uncooled slipper with maximum values of 65°C. The uncooled experiments reveal distinct needle-like peaks that can be related to severe wear. During the last speed plateau, temperatures exceed 130°C. It should also be noted that these high temperatures could affect low speed performance, as already mentioned above. The photos of the surfaces of the slippers after the measurements are shown in the center of Figure 8. The wear pattern reveals, that there is not only particle abrasion (3rd body) but also a smearing effect of the material due to the high temperatures during contact. This mixed friction occurred after the surface temperature of the disc exceeded 100°C, indicating that the oil performance was degraded to a point where insufficient load holding took place. This oil degradation is evident by the pitch-black oil leaking out of the slipper gap, as shown in the photo on the right side in Figure 8.

While the slipper with the step and waved design experienced excessive wear, the multi-land slipper, which is directly taken from the standard series pump, experienced little to no wear in the same test set up. This design is characterized by multiple lands, adding one inner and one outer stabilizing land to the center sealing land. It is widely used as industrial standard and described in more detail f.e. in [24]. The results can be seen in the next figure. Additional to the temperature of the multi-land design without cooling, **Figure 9** also shows the step slipper with and without cooling. It is very interesting to see, that the un-cooled multi-land slipper exhibits a similar behavior to the cooled step slipper.

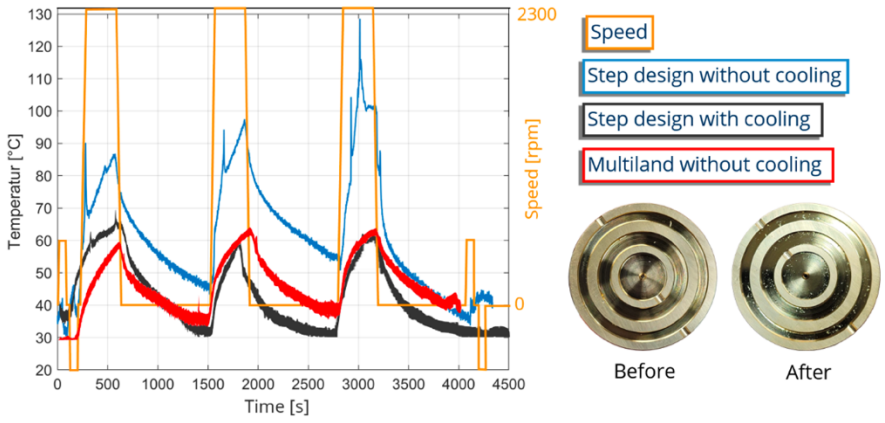

Figure 9: Temperature development for step (with and without cooling) vs. multi-land slipper (without cooling)

5.2. Pump measurements at increased inlet temperature

To investigate the influence of higher temperatures on the pump set-up, steady state measurements at increased inlet temperature as well as an elevated temperature endurance test has been carried out. The former is presented in **Figure 10**, showing the influence of the temperature on the pump losses. The left plot shows the measured torque losses for four different operating conditions at different pressures and speeds over the rising inlet temperature from 35 to 55 °C. All curves show a global reduction in friction losses. The right plot provides the detailed efficiencies of 500 rpm and 350 bar (low speed, high pressure). The hydromechanics efficiency is staying relatively constant while the volumetric efficiency is dropping significantly because of the lower viscosity at higher temperatures.

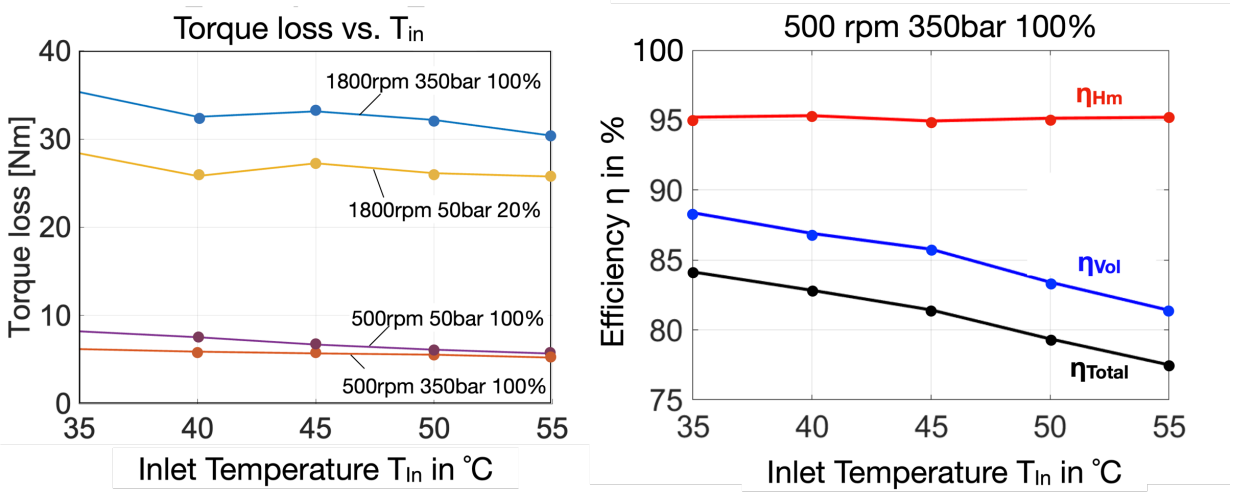

Figure 10: Influence of temperature on the pump losses. Left: Measured torque losses for 4 different operating conditions. Right: Measurement vs. simulation for low-speed high pressure.

Furthermore, an endurance test lasting 565 hours can be provided. Different materials and designs are subjected to a cyclic elevated pressure test in a pump at nominal speed. The combination of increased pressure of over 350 bar and cyclical speed changes results in an estimated temperature increase of over 70°C throughout the system. As shown in **Figure 11** (right), different materials and designs are used for the nine slippers. The profilometric diagrams in Figure 11 (left) allow a quantitative analysis. On average, the lead-free slipper achieves the lowest wear with a maximum of 1 µm on the inner radius. The diamond hardened brass slipper also performs well, but the inner edge wears more. The brass slipper shows the most wear, up to 1.5 µm on the inner radius. It is also interesting to note that the inner ring of the lead-free slipper runs in flat, whereas the brass slipper has

a run-in plane that slopes down towards the inner edge. This may suggest a variation in pressure deformation caused by differences in elasticity moduli, which will be further examined.

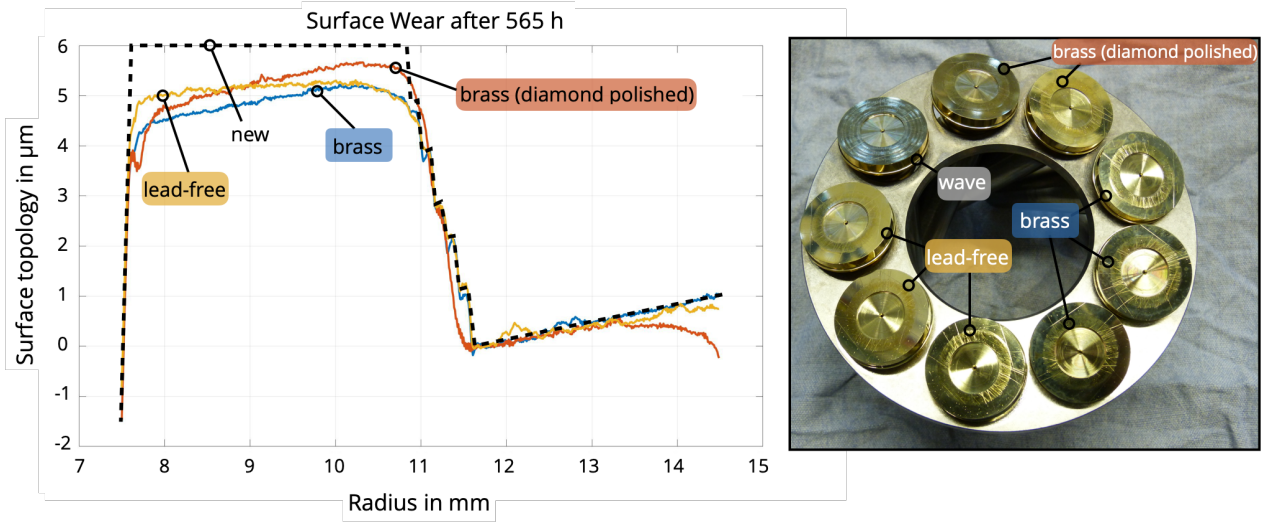

Figure 11: Surface topology of different materials of the step design after endurance testing over 565 hours (left), photo of slipper surfaces after endurance testing (right)

These trends differ to the tribometer results. Therefore, another reason apart from the maximum temperature must be responsible for the different behavior of the slippers. In the following, the temperature deformations for different maximum temperatures and temperature *gradients* in the slippers are analyzed by FEM simulations.

5.3. Simulation of the slipper deformation

To study the deformations on a basic level a simplified ANSYS® model was created that allows an independent investigation of the temperature and pressure deformation and their effect on slipper wear. As the pressure field of the step slipper is quite complex and only the deformation trends are of main interest, the reference design of the slipper was chosen to model using hexahedra elements of quadratic order, compare **Figure 12** (a). It is connected with a spherical joint to the piston that has a fixed support on the bottom as illustrated in Figure 12 (b). The boundary conditions to calculate the pressure and temperature deformation are given in Figure 12 (c).

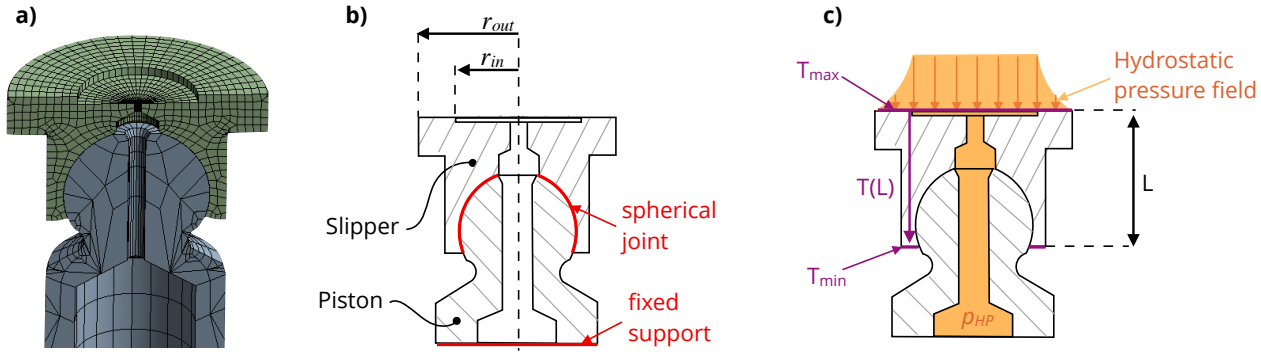

Figure 12: slipper and piston mesh (a), boundary conditions (b) and pressure and temperature loads (c)

For the reference slipper a logarithmic pressure drop can be assumed between the slipper and disc, which decreases over the sealing land from r_{in} to r_{out} up to the atmosphere pressure shown in (1) and derived in [25]. The piston as well as the orifice in the slipper and the slipper pocket are pressurized with p_{HP}.

$$p_{hydrostatic} = p_{HP} \frac{\ln\left(\frac{r}{r_{out}}\right)}{\ln\left(\frac{r_{in}}{r_{out}}\right)} \tag{2}$$

The heat causing slipper deformation originates in the gap between slipper and swashplate. Especially if the gap is very small, mixed friction arises and produces additional heat. Therefore, the maximum temperature is defined on the sealing surface of the slipper. The minimum temperature is assumed to be on the slipper's bottom and is estimated or derived from the simulation results of the pump simulation with Caspar FSTI. The heat transfer is described by the Fourier law and can be used to calculate the temperature distribution T(L) in the slipper.

The critical operating condition of the tribometer is simulated with 200 bar pressure and 130 °C on the slipper surface at a temperature of approx. 50 °C on the slipper bottom. **Figure 13** presents the simulation results with a magnification of the deformation.

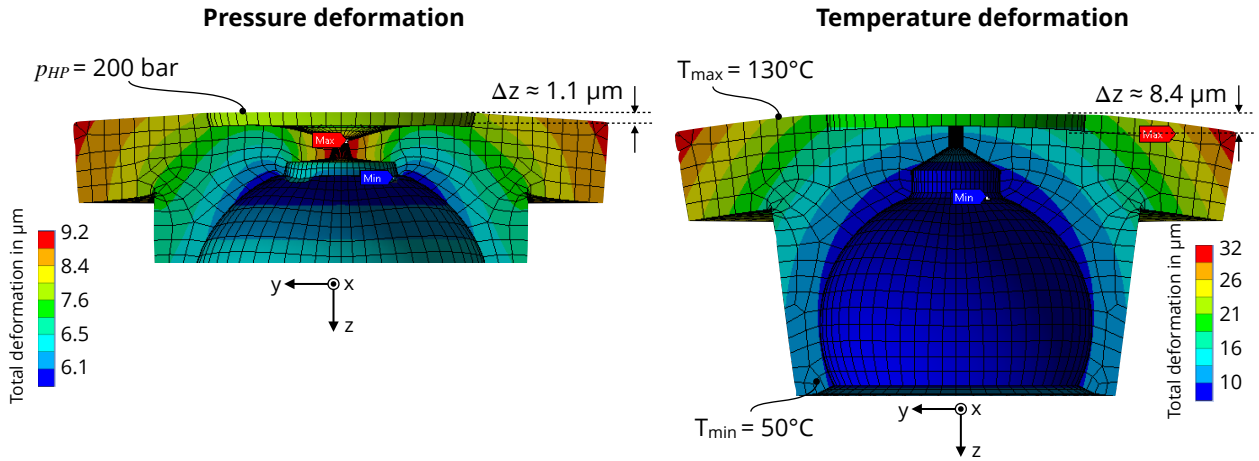

Figure 13: pressure (left) and temperature (right) deformation of the slipper

In the left side of Figure 13 simulation results of the pressure deformation for 200 bar are shown. The colors describe the total deformation of the slipper in all axis. The slipper surface deforms convex with a total radial change in z-direction of about 1.1 µm. Due to the contact conditions between piston and slipper the simulation results are not valid in the lower area of the slipper opening. In reality the edge of the slipper widens and the gap opens locally.

In the right side of Figure 13 the simulation results of the temperature deformation for 130 °C at the slipper surface are shown. The deformation is also of convex shape with a total radial change in z-direction of about 8.4 µm, which is significantly greater compared to the pressure influence. **Figure 14** shows the deformation in z-direction over ΔT (T_{max} -Tmin across the slipper) for different maximum temperatures 70, 100 and 130 °C. The surface deformation is greatly influenced by the temperature gradient, while the maximum surface temperature has no effect. This mathematical relationship can be derived from the linear thermal expansion equation, with ΔL as change in length, L as total length and α as thermal expansion coefficient.

$$\Delta L = \alpha \cdot \mathrm{L} \cdot \Delta \mathrm{T} \tag{3}$$

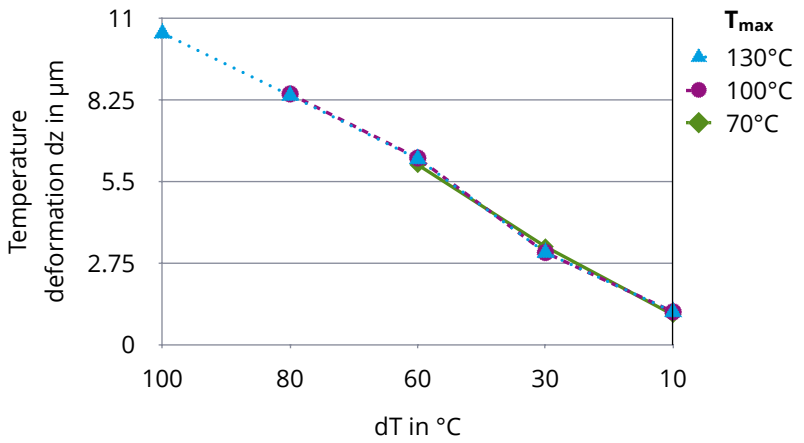

Figure 14: temperature deformation in z-direction over the temperature gradient for different maximum temperatures

5.4. Conclusion of the thermal behaviour of the step slipper

The experiments described were used to test the thermal limits of the step design, which appears to behave unfavourably at high temperature gradients, e.g. very high temperatures in the gap while surrounded by cooler oil and air. This is due to the convex temperature deformation of the slipper surface, which is quantified in the simulation section. The additional material of the step in the inner ring is counterproductive during such deformation.

This theory was confirmed by the tribometer and pump measurements. The differences of the thermal boundary conditions between the set-ups seem to be crucial. The tribometer set-up allows for different cooling arrangement. Without any cooling the slipper moves in an oil-free surrounding, providing little-to no convective cooling, as the slipper itself does not move. In the pump the slipper rotates through the case oil, which is typically warmer than the inlet and outlet temperature of the pump. Any heat generation in gaps will be dissipated into the case, while simultaneously preheating all parts to a homogenous temperature. In the tribometer the lack of case oil allows the individual parts to have significantly different temperatures, as the air surrounding the parts thermally insulates them from each other. In addition, the parts have a much higher thermal gradient, as the surround air is at room temperature always, while warm oil enters the slipper and increases significantly in the gap.

The multi-land slipper appears to be more tolerant to uneven thermal loading compared to the step design. This can be mainly explained by the fact that the amount of leakage for the multi-land slipper is clearly higher than for the step slipper. This is shown by the efficiency graphs in **Figure 15** in Appendix A, providing pump measurement results over a large set of pressure and speeds values. Additionally, it is assumed that the grooves of the multi-land slipper work as a kind of cooling channels. As the leakage oil has no direct path but has to exit through the dedicated openings on the outer sealing land. This also means that the leakage oil stays in contact with the slipper for a longer time as compared to the single land slipper, where it has a more direct leakage path. This suggests that the multi-land slipper may be a more suitable option than the step slipper for certain applications like dry-case operation, in which the case oil is drained to reduce churning losses.

6. CONCLUSION AND OUTLOOK

This paper presents a hydrostatic tribometer designed to evaluate slipper performance in various scenarios, which are challenging to test in full pump tests. Unlike earlier hydrostatic tribometers, this model uses unaltered original pump parts integrated into a commercial disc-on-disc tribometer. It features an external pressure source and operates with stationary components (block, piston, and

slipper) and a moving swash plate. While it reduces the physical representation of a pump, its focused study on the behaviour of interchangeable slipper designs under specific conditions is beneficial.

Previous results of the innovative step-design on the pump test rig were promising [2], yet some measurement results were difficult to explain even using the advanced simulation tool Caspar FSTI. Particularly notable were the differences in wear levels during high-speed, high-pressure, and high-temperature endurance tests compared to steady-state measurements, which included low speeds and varying conditions. The increased wear in the latter, despite significantly reduced torque losses with the step design, suggested transient conditions as a cause, particularly thermal transients not captured by the simulation tool, which is limited to thermal steady states. The tribometer's low-speed performance evaluations of slipper designs showed trends and magnitudes comparable to pump test rig results. However, increasing pressure created a misleading impression of the step design's inferiority, contrary to pump environment observations. This discrepancy underscores the limitations of tribometers, such as the absence of centripetal force and pressure permutation, which can yield differing results under pressurized conditions. Nonetheless, the findings offered valuable insights into slippers' complex behaviours, particularly in low-pressure scenarios at low speeds.

The thermal boundary conditions in the tribometer are significantly different compared to the regular pump. The slipper and swash plate, not submerged in oil and surrounded by room temperature, exhibit a reduced convection coefficient, especially due to the lack of rotational movement of the slipper. To allow for a better heat dissipation an active cooling system was installed. It blows cold air and sprays oil at room temperature onto the swash plate and slipper. Turning off or adjusting this system allows to test in different thermal boundary conditions. Pump tests and simulations indicated improved slipper torque losses with rising inlet oil temperature, contrasting the presented tribometer results. When the cooling system was turned off there was a significant thermal strain on the slipper with temperature exceeding 130˚C, which lead to black leakage oil and significant slipper wear. However, even with the cooling system turned on, the wear patterns were not matching the pump testing. It was concluded that the high temperature gradient from >100˚C in the gap to surfaces sprayed with cold oil and air caused a higher than usual thermal deformation leading to wear and increased torque readings. This behavior was confirmed by FEM simulations, illustrating that high thermal gradients increase the deformation significantly. Unfortunately, this thermal wear is a self-amplifying process, where higher temperature led to more wear, which lead to even higher local temperatures. The results indicate the need for slippers to operate in a more uniform temperature field to minimize wear. This is achieved when submerging the slipper with leakage oil, which will lead to a smaller temperature gradient even at elevated temperatures.

The shown findings emphasize the complexity of pumps and their components. Changing just one boundary condition could alter the performance drastically. The hydrostatic-tribometer has shown its merits when testing different designs in defined ramps and conditions. However, the resulting trends cannot be projected into the pump environment, as too many variables have changed. Especially the different thermal conditions have shown to be a major factor for this discrepancy. One step further to a comparable pump set-up would be to allow the slipper to run through oil and to establish a homogeneous temperature throughout the sliding parts. Further investigations will involve material studies including a lead-free and a steel slipper.

In conclusion, it can be said that the results give a deeper insight into the complex physical phenomena that slippers exhibit and can be used to test for limits of operation and thermal behaviour. These insights are vital for understanding and optimizing pumps, especially in the context of electrification and the need to test critical speed levels, maximum allowed acceleration, and thermal limits.

7. ACKNOWLEDGEMENTS

The presented research activities are part of the project “Tribologieoptimierung von Pumpensystemen durch fertigungsgerechte Einbringung von Mesostrukturen” (Ref. No. 20757 BR/1). The authors would like to thank the Fluid Power Research Fund of the VDMA for the funding and support.

NOMENCLATURE

α	Thermal expansion coefficient	1/K
B	Balance	%
β	swashplate angle	°
F_{fz}	Hydrostatic force	N
F_{AK}	Piston force	N
L	length of the slipper	mm
p	pressure	bar
r	radius	mm
T	Temperature	°C
ΔT	Temperature difference	K
Δz	Deformation in z-axis	µm

APPENDIX A

Figure 15 displays the volumetric (left) and hydromechanics (right) efficiency graphs of pump measurement results over several pressure blocks from 50 to 300 bar within each speeds from 500 to 1500 rpm are measured. The single measured efficiency values are connected by lines to better visualize the differences of the designs. The purple curve represents the multi-land efficiencies in both graphs, which are lower than the step and the reference efficiencies for all operating conditions concerning the volumetric losses. This supports the theory that the multi-land design produces more leakage that is helping to cool the slipper, reducing the deformation due to temperature and thus preventing contact and wear. As the hydromechanic efficiency of the multi-land slipper is quite good especially for higher pressures, the overall performance of the multi-land slipper is as good as the step slipper for 300 bar and 1-2 percentage points worse for lower pressures. The pump measurements also have shown, that the efficiency advantage of the step slipper over the multi-land slipper even increases for lower swashplate angles due to stabilizing effects of the micro-structure described in more detail in [3].

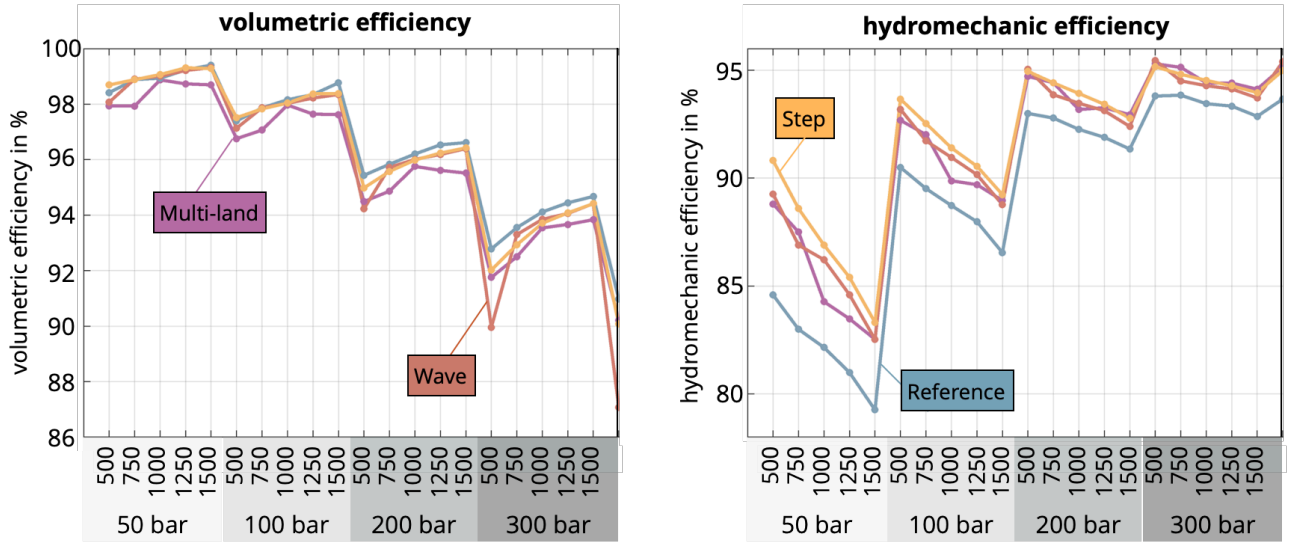

Figure 15: Volumetric and hydromechanic efficiency for different slipper designs and OCs

REFERENCES

1. Ivantysynova M, Baker J (2009) Power loss in the lubricating gap between cylinder block and valve plate of swash plate type axial piston machines. Int J Fluid Power 10:29–43. https://doi.org/10.1080/14399776.2009.10780976
2. Horn S, Ivantysyn R, Weber J (2022) Validated efficiency improvements by implementation of structures on the slipper surface of an axial piston pump. IEEE GFPS 2022
3. Horn S, Ivantysyn R, Weber J (2022) Tribo-optimized lubricating interfaces in hydrostatic pumps with surface shaped slippers. IFK2022
4. Ivantysyn R, Horn S, Weber J (2022) Design of a Lead-Free Slipper Bearing for Low Speed Axial Piston Pump Applications. IEEE GFPS 2022
5. Haidarschin G, Hesebeck M, Su E, Diesselberg M (2018) Benchmarking of potential substituents for leaded bronze in axial sliding bearings for mobile hydraulic applications. Fluid power networks Proc 19th - 21th March 2018 11th Int Fluid Power Conf 54–67
6. Manring ND, Wray CL, Dong Z (2004) Experimental studies on the performance of slipper bearings within axial-piston pumps. J Tribol 126:511–518. https://doi.org/10.1115/1.1698936
7. Renius KT (1973) Experimentelle Untersuchung an Gleitschuhen von Axialkolbenmaschinen. O + P Zeitschrift für Fluidtechnik 17:75–80
8. Canbulut F, Sinanoğlu C, Koç E (2009) Experimental analysis of frictional power loss of hydrostatic slipper bearings. Ind Lubr Tribol 61:123–131. https://doi.org/10.1108/00368790910953631
9. Hooke CJ, Kakoullis YP (1978) The Lubrication of Slippers in Axial Piston Pumps. In: 5th Fluid Power Symposium
10. Bergada JM, Haynes JM, Watton J (2008) Leakage and Groove Pressure of an Axial Piston Pump Slipper with Multiple Lands. Tribol Trans 51:469–482. https://doi.org/10.1080/10402000802044332
11. Rizzo G, Massarotti GP, Bonanno A, et al (2015) Axial piston pumps slippers with nanocoated surfaces to reduce friction. Int J Fluid Power 16:1–10. https://doi.org/10.1080/14399776.2015.1006979
12. KAZAMA T, TSURUNO T, SASAKI H (2008) Temperature Measurement of Tribological

Parts in Swash-Plate Type Axial Piston Pumps. Proc JFPS Int Symp Fluid Power 2008:341–346. https://doi.org/10.5739/isfp.2008.341

13. Tang H sheng, Yin Y bao, Zhang Y, Li J (2016) Parametric analysis of thermal effect on hydrostatic slipper bearing capacity of axial piston pump. J Cent South Univ 23:333–343. https://doi.org/10.1007/s11771-016-3078-0
14. Lin S, Hu J (2015) Tribo-dynamic model of slipper bearings. Appl Math Model 39:548–558. https://doi.org/10.1016/j.apm.2014.06.009
15. Hooke CJ (1983) The effects of non-flatness on the performance of slippers in axial piston pumps. Proc Inst Mech Eng Part C J Mech Eng Sci 197:239–247. https://doi.org/10.1243/PIME_PROC_1983_197_104_02
16. Wang X, Yamaguchi A (2002) Characteristics of hydrostatic bearing/seal parts for water hydraulic pumps and motors. Part 1: Experiment and theory. Tribol Int 35:425–433. https://doi.org/10.1016/S0301-679X(02)00023-3
17. Iboshi N, Yamaguchi A (1982) Characterisitics of a Slipper Bearing for Swash Plate Type Axial Piston Pumps and Motors. Bull JSME 2091
18. Chao Q, Wang Q, Xu B, Chen Y (2017) Experimental verification of slipper spinning motion in axial piston pumps. In: Proceedings of the ASME/BATH 2017 Symposium on Fluid Power and Motion Control FPMC2017. pp 1–7
19. Chao Q, Zhang J, Xu B, et al (2019) Test rigs and experimental studies of the slipper bearing in axial piston pumps: A review. Meas J Int Meas Confed 132:135–149. https://doi.org/10.1016/j.measurement.2018.09.027
20. Chao Q, Zhang J, Xu B, et al (2019) Test rigs and experimental studies of the slipper bearing in axial piston pumps: A review. Meas J Int Meas Confed 132:135–149. https://doi.org/10.1016/j.measurement.2018.09.027
21. Horn S, Ivantysyn R, Schneider J, et al (2022) Tribologieoptimierung von Pumpensystemen durch fertigungsgerechte Einbringung von Mesostrukturen. Dresden, Germany
22. Renius KT (1972) Zum Entwicklungsstand der Gleitschuhe in Axialkolbenmaschinen 1. O + P Zeitschrift für Fluidtechnik 16
23. Shorbagy A, Ivantysyn R, Berthold F, Weber J (2022) Holistic analysis of the tribological interfaces of an axial piston pump - Focusing on pump ’ s efficiency. In: IFK2022. Aachen
24. Renius KT (1972) Zum Entwicklungstand der Gleitschuhe in Axialkolbenmaschinen. Ölhydraulik und Pneum 16:494–497
25. Hamrock BJ, Schmid SR (1991) Fundamental of Fluid Film Lubrication